Parallax indicates simple cue-anchoring in the head-direction system

Sven Krausse
Forschungszentrum Jülich - PGI 15
RWTH Aachen University - Institute for Electrical Engineering and Information Technology
Aachen, Germany
s.krausse@fz-juelich.de

Adrian J. Duszkiewicz
University of Stirling - Division of Psychology, Faculty of Natural Sciences
Stirling, United Kingdom

Emre Neftci
Forschungszentrum Jülich - PGI 15
RWTH Aachen University - Institute for Electrical Engineering and Information Technology
Aachen, Germany

Friedrich T. Sommer
UC Berkeley - Redwood Center for Theoretical Neuroscience, Berkeley, USA

Alpha Renner
Forschungszentrum Jülich - PGI 15, Aachen, Germany
a.renner@fz-juelich.de

Abstract

The rodent head-direction (HD) system provides an internal compass for spatial navigation by integrating angular head velocity and anchoring to visual landmarks. A fundamental challenge for this computation is parallax: as the animal moves, the direction of nearby landmarks shifts, potentially introducing systematic, position-dependent errors. Whether and how the HD system corrects for parallax has remained unclear. Here we show that the HD signal in the postsubiculum of freely moving mice exhibits position-dependent biases consistent with parallax in a single-cue environment. These biases were smaller than predicted by geometric calculation of parallax, and in more natural, multi-cue settings the bias was strongly attenuated. Using computational modeling, we further show that two passive effects are sufficient to explain this attenuation: multi-view averaging, whereby temporal integration of the same landmark sampled from different locations averages out position-dependent error, and multi-cue averaging, whereby concurrent weighting of multiple landmarks causes their parallax-induced biases to cancel each other out. Our results suggest that passive averaging, without active position-dependent correction, provides a simple and robust strategy for maintaining a stable allocentric reference frame, central to cognitive mapping. More broadly, these findings highlight a trade-off in neural coding between computational efficiency and positional accuracy, with implications for both biological and artificial navigation systems.

Keywords: navigation; postsubiculum; parallax; sensory integration; head-direction cells; bearing cells; landmark anchoring

Main

Accurate spatial navigation depends on a reliable sense of direction. The head-direction (HD) circuit is a canonical component of the brain's spatial positioning system across diverse animal lineages (Rank, 1984; Taube et al., 1990a; Kim & Maguire, 2019; Petrucco et al., 2023). In mammals, it consists of HD cells - neurons that fire when the animal faces a specific direction in the global (allocentric) reference frame, and whose collective activity constitutes an internal compass (Taube, 2007). This compass is crucial for downstream spatial codes, including grid cells in the medial entorhinal cortex (Winter et al., 2015) and hippocampal place cells (Harland et al., 2017).

The HD signal originates in the dorsal tegmental nucleus (DTN) and lateral mammillary nucleus (LMN). It is relayed through the anterior thalamus (Mizumori & Williams, 1993; Taube, 1995) to the postsubiculum (PoSub) (Rank, 1984; Taube et al., 1990b; Duszkiewicz et al., 2025) to be broadcast to higher-order cortical navigation systems. Angular head velocity (AHV) inputs update the HD signal through temporal integration (McNaughton et al., 1991, 2006; Taube, 2007; Bassett & Taube, 2001; Sharp et al., 2001). However, because AHV integration alone accumulates drift, stable orientation requires anchoring to visual landmarks (Taube et al., 1990a; Goodridge et al., 1998; Knierim et al., 1995; Zugaro, Berthoz, & Wiener, 2001; Zugaro et al., 2003). As visual inputs are inherently egocentric, they first must be transformed into an allocentric reference frame (Skaggs et al.,

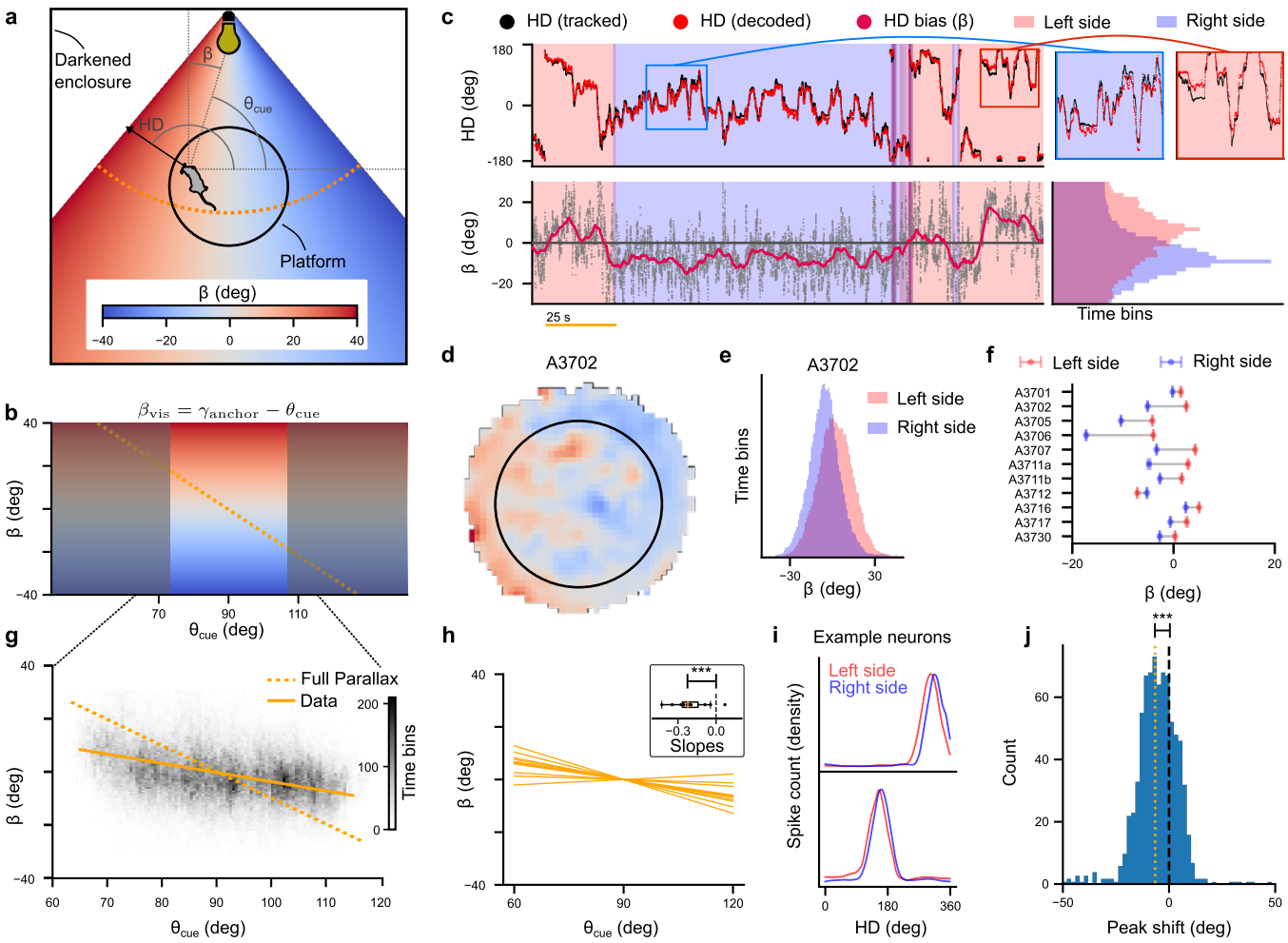

Figure 1: **Position-dependent parallax error in head direction (HD) estimation.** (**a**) Sketch of experimental setup. Parallax-induced HD bias β color-coded at different locations in the arena. Cue azimuth θ_{cue} and expected HD bias β are indicated in gray. Orange trajectory shows a line of linear change in expected HD bias, as shown in panel (b). (**b**) Expected linear relationship between the parallax-induced HD bias β and the Cue azimuth θ_{cue}. In panel (g), we can therefore perform linear regression to estimate the strength of the parallax effect using the equation at the top with $\gamma_{anchor} = 90°$ as the offset between the two angles. (**c**) Example data from Duszkiewicz et al. (2024) showing the parallax effect in raw traces. Top panel shows tracked (black) and decoded (red) HD. Inset plots on the right show a zoomed-in version of two examples where the systematic HD bias is visible. Bottom panel shows the difference between the tracked and decoded HD. We color-code the background of the plot to indicate whether the animal is towards the right (blue) or left (red) of the cue. The vertical histogram on the bottom right shows the distribution of recorded HD bias split by the animal being on the right/left side of the cue. (**d**) Heat map of the measured HD bias β across the platform. Color indicates the mean recorded HD bias for each pixel in the environment (same color map as in panel (a)). (**e**) Histogram of measured HD bias in a single recording session. The two histograms correspond to time points where the animal is either on the left (red) or right (blue) side of the circular platform. (**f**) Plotted mean HD bias for each session when the animal is on the left/right side of the cue. Error bars indicate the error on the mean. (**g**) Measured HD bias (difference between tracked and decoded HD) vs. object angle θ_{cue}. Linear regression line is shown in orange and shows a significantly non-zero slope (see panel (h) for all linear regression results and slopes). (**h**) Plot of linear regression lines for all 11 sessions. Inset shows a box plot of the distribution of computed slopes in the linear regression. The distribution clearly indicates that the slopes are significantly below zero (One-tailed t-test, $p = 9 \cdot 10^{-4}$, Cohen's $d = -1.30$), as expected by the parallax effect. (**i**) Tuning curves of two example neurons. Tuning curves are computed on two subsets, when the animal is either on the left (red) or right (blue) side of the cue. A shift in the peak is detectable even on this single neuron level (see also panel (j)). (**j**) Distribution of peak shifts for all neurons of all sessions. We compute the peak in the cross-correlation between the two tuning curves shown in panel (i) for each neuron in each session to determine how much the two tuning curves are shifted in each neuron. The resulting distribution shows that the neurons have a significant tendency to be negatively shifted (One-tailed t-test, $p = 1.4 \cdot 10^{-5}$, Cohen's $d = -0.15$), indicating a parallax effect that can be measured even on the single neuron level.

1994; Zhang, 1996; Hahnloser, 2003; Bicanski & Burgess, 2016; Boucheny et al., 2005). This transformation introduces a challenge: nearby cues shift in egocentric bearing as the animal moves even when keeping a constant head direction, a phenomenon known as the parallax effect. This should impose systematic, position-dependent errors unless corrected. To date, it remains unresolved how the HD circuit accurately integrates egocentric cues to maintain a stable allocentric reference frame.

Prevailing models of the HD system either disregard the parallax effect by assuming landmarks are infinitely distant (Skaggs et al., 1994; Zhang, 1996; Hahnloser, 2003; Boucheny et al., 2005), or propose explicit position-dependent corrections via hippocampal place cells (Bicanski & Burgess, 2016). The latter potentially introduces a circular dependency, as place cells are thought to rely on a stable HD signal (McNaughton et al., 2006; Burak & Fiete, 2009). Thus, despite decades of research, and strong evidence for landmark anchoring (Taube et al., 1990a; Goodridge et al., 1998; Knierim et al., 1995; Zugaro, Berthoz, & Wiener, 2001; Zugaro et al., 2003), it remains unknown how the HD system anchors to finite-distance landmarks without introducing parallax errors.

Here, we show that the PoSub HD signal indeed exhibits a systematic, position-dependent bias, consistent with parallax, when anchored to a single visual landmark. The magnitude of this bias was smaller than predicted by simple geometry. Modeling shows that parallax can be strongly attenuated via two passive mechanisms, without requiring active position-dependent correction: first, multi-view averaging, in which temporal integration of the same landmark across different locations reduces position-dependent errors; and second, multi-cue averaging, in which concurrent weighting of several landmarks causes their individual parallax biases to cancel. Importantly, the spatial pattern of the bias can be informative about the assumed anchoring angle between egocentric landmark bearing and head direction.

Results

HD signals exhibit parallax error in a single-cue environment

We first tested whether the head-direction (HD) signal is distorted by parallax in a single-cue environment. We recorded large populations of PoSub HD cells while mice freely explored an elevated circular platform (n = 823 HD cells; 11 sessions from 10 mice) and tracked the animal's head direction using high-definition motion capture (Methods, Duszkiewicz et al. (2024)). The platform was placed inside a darkened enclosure designed to minimize the availability of uncontrolled visual cues. The only light source within the enclosure was a dim LED cue mounted on one wall, visible from the platform but inaccessible to the animal (Fig. 1a, see Methods). If the HD system fully corrects for parallax in this paradigm, the decoded HD should be independent of the animal's location on the platform. In contrast, if the HD signal is subject to parallax, HD should be offset depending on the (allocentric) cue azimuth θ_{cue} (Fig. 1a,b).

To disambiguate between these two possibilities, we decoded the internal HD signal from PoSub spiking activity with a Bayesian decoder (Methods) and computed the HD bias β_{dec} as the difference between the decoded HD and the motion-capture HD in the global reference frame (Fig. 1c). Surprisingly, we observed a systematic dependence of HD bias on cue azimuth, consistent with parallax (Fig. 1d). When the animal was on the right side of the platform, we observed a negative HD bias, whereas positions on the left side showed positive bias (Fig. 1c-f). All eleven sessions exhibited highly significant differences in mean HD bias between left and right conditions (Fig. 1f; Welch's t-tests, all $p < 0.001$; Suppl. Tab. 1). In 10 of 11 sessions, the bias was positive when on the left side of the platform compared to negative on the right (Cohen's $d = 0.13$ to 1.16, median $|d| = 0.34$), indicating that the HD signal is subject to parallax error in a single-cue environment.

To quantify the amount of parallax, we used linear regression between the HD bias β_{dec} and the cue azimuth θ_{cue} (Fig. 1c, Equations (3)-(6) in Methods). In this framework, the slope of the regression (w) denotes the amount of parallax. $w = -1$ corresponds to maximal parallax, i.e., purely visual cue-based orientation and $w = 0$ to full parallax correction. We call the x-intercept of the linear regression *anchoring angle* (γ_{anchor}) - the direction that defines the alignment of the HD signal with respect to the cue. This cue–HD alignment is also implied by landmark-control experiments, in which rotating a salient cue rotates preferred directions of HD cells with a fixed offset (Taube et al., 1990a; Goodridge et al., 1998; Zugaro et al., 2003). To account for the possibility of different anchoring angles across animals and session, the fit was performed separately for each session (Fig. 1h). We observed fitted slopes significantly below zero in 10 out of 11 recording sessions (weighted mean slope $\overline{w} = -0.23 \pm 0.008$), meaning that the parallax effect was apparent in all but one session (bootstrapped t-test, p-values < 0.05, Methods, Suppl. Tab. 3). However, the maximal negative measured slope was -0.43, indicating a lower position dependence of the systematic error than the $w = -1$ predicted by simple geometry. To exclude the possibility that these findings on the population level are an artifact resulting from biases in the tuning curves of a few neurons, we repeated the analysis where we constrained the tuning curve estimation to time intervals where the animal was in the center of the environment. All findings presented above could qualitatively be reproduced (see Suppl. Sec. Analysis of tuning curves from only the center of the environment).

Given that the parallax error was reliably detected at the population level, we next asked whether it is also expressed at the level of individual HD cells. Establishing this is important because a population-level bias could, in principle, be driven by a small subgroup of neurons with idiosyncratic tuning, or by decoding-related artifacts. If, however, parallax affects the tuning of single HD neurons, their preferred firing direction should shift systematically with the animal's cue azimuth. To

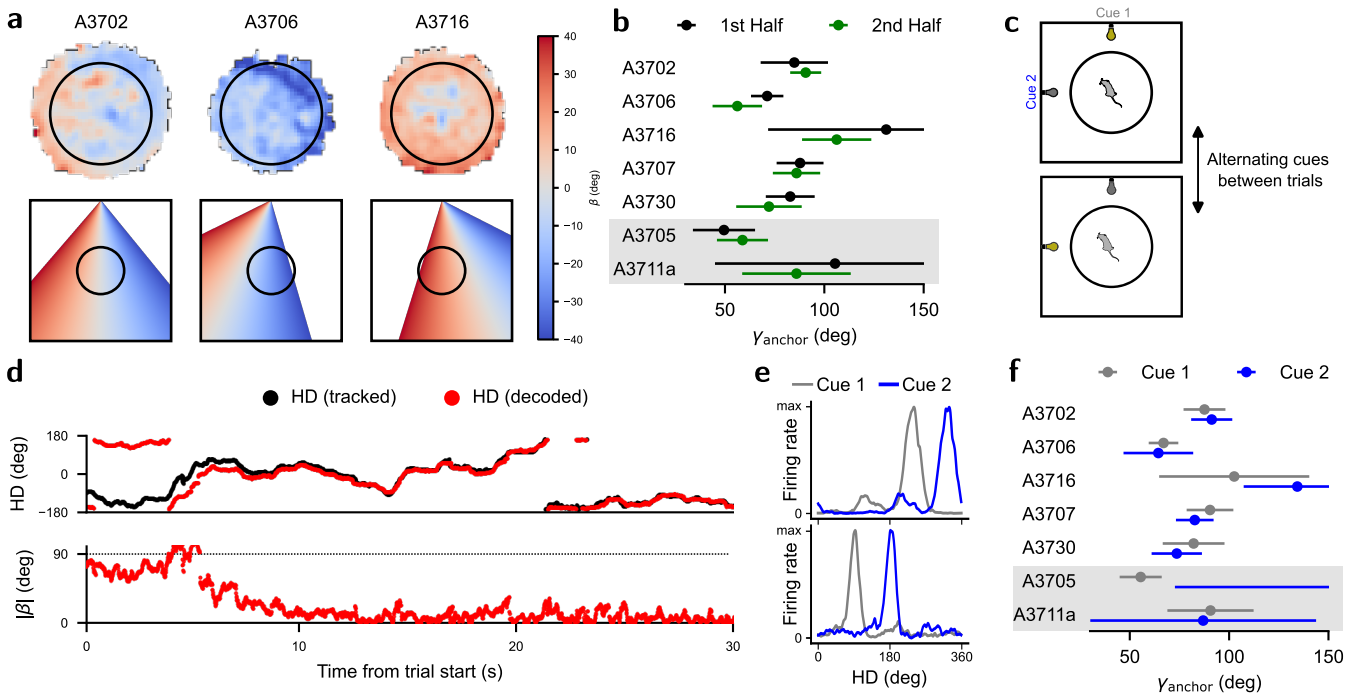

Figure 2: **Estimating the anchoring angle γ_{anchor} based on parallax effects.** (**a**): Top panels: Heat maps of the animal during three different recording sessions, color-coded by the observed angular error β_{dec} of the neural data at each location. Bottom panels: Theoretical predictions of the spatial distribution of β from a purely vision-based HD model. (**b**): Anchoring angles for included sessions from the single-cue dataset, as computed from the linear regression results (Eq. 7). Anchoring angles are computed for the first and second halves (split over time) separately. Note that the first five sessions in this plot were sessions that exhibited reorientation after the cue switch occurred, while the bottom two sessions (*A3705* and *A3711A*, grey background) did not show reorientation. (**c**): Illustration of cue switching between different trials of a recording session. Between each trial, the position of the single cue was changed to the center of a different wall, then throughout the recordings, the two cues were presented alternatingly over the course of 16 trials (8 per cue). (**d**): Example trace of the first 30 seconds after a trial start. After an adaptation period, the decoded HD shifts to the 90-degree rotated cue. (**e**): Two example tuning curves of a neuron in the two different cue conditions. The preferred firing direction shifts in the two different cue conditions by the amount of rotation of the cue (90 degrees). (**f**): Anchoring angles computed for the seven sessions in the two different cue conditions. The anchoring angles for the original and rotated cues indicate that the anchoring angle remains relatively stable over time and across rotations of the cue.

test this, we split the sessions into two conditions depending on whether the animal was on the left or right side of the platform. We computed HD tuning curves separately for left and right conditions (Fig. 1i) and quantified the shift between the two tuning curves using cross-correlation. We observed a significant clockwise shift of the left-side tuning curves relative to the right-side (mean = $-3.86^\circ \pm 0.88^\circ$, $n = 823$ neurons, $p = 1.35 \times 10^{-5}$, one-sample t-test). The distribution of peak shifts across the full population shown in Fig. 1j indicates that parallax is not restricted to a few outlier cells but instead represents a robust, system-wide property of the HD network.

Parallax errors reveal the anchoring angle

Cue-control experiments show that salient landmarks can quickly gain control over the head-direction (HD) signal, implying that the system learns a fixed alignment between (egocentric) cue bearing and its internal compass (Taube et al., 1990b; Goodridge et al., 1998; Zugaro et al., 2003). The *anchoring angle*, γ_{anchor}, introduced above, captures this alignment. Defined as the x-intercept of the bias-azimuth regression, it marks the cue azimuth where parallax errors vanish. This makes the spatial pattern of parallax errors a useful measurement tool for estimating how the HD representation is anchored to visual landmarks.

Intuitively, γ_{anchor} can be thought of as the head direction at which landmark control was first established, i.e., the "anchoring event". When the landmark reappears after a period without it, the system should tend to correct its internal compass back toward this offset. In principle, differences in γ_{anchor} could also be measured by alternating between two distinct cues that are either learned together (no offset expected) or separately (yielding a relative HD shift corresponding to the

difference in anchoring angles).

To estimate γ_{anchor} from the data, we examined the spatial distribution of parallax errors across animals. We observed distinct spatial patterns of HD bias in individual recordings (Fig. 2a, Suppl. Fig. 11), suggesting that γ_{anchor} is session-specific. We quantified this by fitting the linear regression between HD bias and cue azimuth and identifying the cue direction at which the bias crossed zero (the x-intercept). Because this estimate is sensitive to noise, we restricted the analysis to sessions with consistent linear relationships (standard deviation of slope $w < 30^\circ$, $n = 7$ sessions).

The resulting γ_{anchor} estimates were stable within sessions, showing agreement between the first and second halves of each recording (Fig. 2b). Across sessions, γ_{anchor} clustered within about 40° of the platform center, consistent with anchoring occurring when the cue lies within the mouse's field of high visual acuity (van Beest et al., 2021).

We further tested the stability of γ_{anchor} during cue rotations (Fig. 2c). In each recording session the location of the LED cue was switched between trials, alternating between two adjacent walls of the enclosure. In sessions where the HD system reliably realigned to the rotated cue within seconds (Fig. 2d,e), the estimated γ_{anchor} before and after rotation overlapped within confidence intervals (Fig. 2f, top, $n = 5$). This is consistent with the view that the system treated the rotated cue as the same landmark, maintaining the same anchoring angle. In contrast, in sessions where realignment to the other cue location failed ($n = 2$), γ_{anchor} could not be estimated reliably (Fig. 2f, grey), consistent with the system treating the rotated cue as novel and unanchored.

Together, these findings show that the anchoring angle can be inferred from the spatial structure of parallax errors, indicating that HD anchoring occurs at a specific bearing relative to visual landmarks.

Parallax errors are attenuated in a standard recording environment

In natural settings and most laboratory experiments, animals are surrounded by multiple landmarks. In such conditions, the parallax errors introduced by individual cues could average out, reducing the overall distortion without the need for active correction, which might explain why parallax errors were not observed in previous studies of the HD system (Taube et al., 1990b).

We therefore analyzed additional PoSub recordings from animals foraging in a standard square open-field environment with a single cue card (n = 1041 HD cells; 16 sessions from 16 mice) (Fig. 3a). In contrast to the single-cue paradigm, this environment was illuminated, thereby providing several additional unintentional landmarks, likely including the corners and boundaries of the enclosure. We found that while we still observed a parallax effect relative to the cue card when the cue card was in view, its magnitude was substantially reduced compared to the single-cue paradigm (Fig. 3b-d; Welch's t-test, p-value < 0.001, Suppl. Tab. 2).

We also performed the single neuron tuning curve analysis for this multi-cue data (Fig. 3e,f). The shift between tuning curves was weaker than in the single-cue paradigm but still significant (mean = $-1.16^\circ \pm 0.45^\circ$, $n = 1041$ neurons, $p = 0.011$, one-sample t-test). The shift magnitude differs significantly between the experimental paradigms ($p = 6.55 \times 10^{-3}$, two-sample t-test), confirming the results of the system-level analysis, that multiple cues help correct for the parallax error from each individual cue.

The parallax effect is dependent on cue visibility

In addition to using visual cues, animals rely on integrating self-motion information, which is not subject to parallax. This is most apparent during time intervals with no available visual cues, in which the animal must solely rely on internal information like angular head velocity (AHV). We therefore investigated whether the observed parallax effect disappears when the visual cue is not within the mouse's field of view (out-of-view conditions) in comparison with periods where the animal is directly facing the cue (in-view conditions) (Fig. 3g). We expect to see a difference between the two conditions in the single-cue but not the multi-cue paradigm as the animal can use additional cues for visual position estimation in the multi-cue paradigm, even when the intentionally placed cue-card is out of view.

We indeed observed lower parallax when the cue was behind the mouse and could therefore be assumed to be out of view. In the single-cue paradigm, 10 out of 11 sessions showed a significantly lower regression slope in out-of-view conditions (Suppl. Tab. 3) than when the animal is facing the cue directly (in-view conditions) (t-test p-value < 0.05, Fig. 3h, Suppl. Tab. 2). As expected, the multi-cue paradigm did not show a significant shift between the in-view and out-of-view conditions (Fig. 3h, Suppl. Tab. 2).

In the next section we explore a possible mechanism explaining the reduction of parallax through both, the presence of multiple cues and viewing the same cue from different angles.

Simple integration passively attenuates parallax error

The observed attenuation of the parallax error could, in principle, arise from an active position-dependent mechanism (Bicanski & Burgess, 2016). However, it may also emerge passively through two simpler processes: 1. *Multi-view integration*, where the animal sees the cue from many different view points and integrates these over time, and 2. *Multi-cue integration*, where cues with different parallax average out.

To assess whether the simplest mechanism, basic cue anchoring, as suggested by cue-control experiments and our data, is sufficient to attenuate parallax error, we next provide a minimal model of internal HD generation without any position-dependent corrections.

The HD system is thought to integrate AHV from vestibular and proprioceptive inputs while using visual landmarks to prevent drift (Blair & Sharp, 1996; McNaughton et al., 1991;

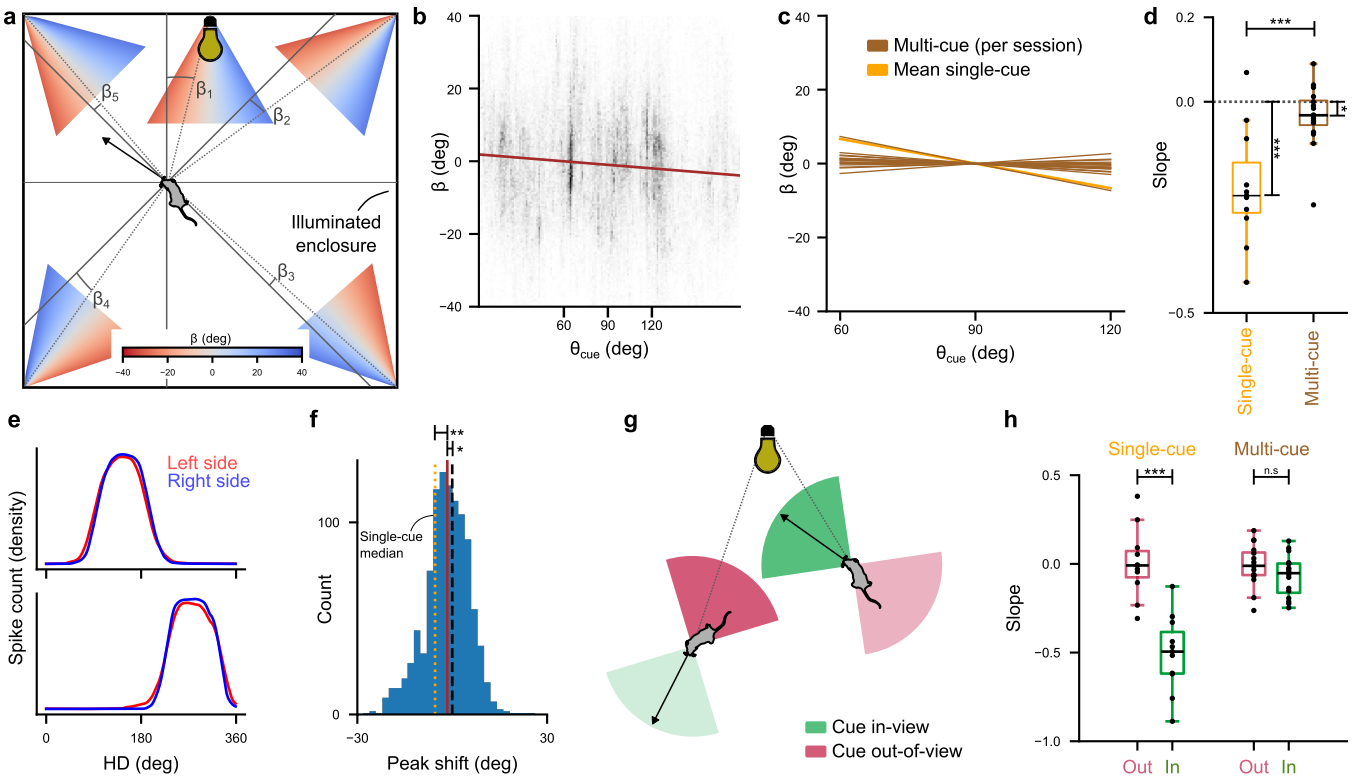

Figure 3: **Reduced parallax effects in a multi-cue environmental setting.** **(a)**: Sketch of experimental setup in multi-cue environment. The animal is navigating in an illuminated environment with a fixed cue on the top wall. Additional features in the room can additionally be used as anchors for the HD system and should therefore have their own parallax error, illustrated by the different color maps. The choice of the four corners as additional cues is merely illustrative - in principle, any additional visual cues could be used to anchor the HD. **(b)**: Example sessions linear regression results. Relationship between the azimuth to the cue card θ_{cue} and the observed HD bias β_{dec}. Individual data points are calculated from the decoded HD traces; the brown line indicates the fitted linear regression. The range of θ_{cue} is determined by the size of the environment. **(c)**: Linear regression lines for all 16 recording sessions in the multi-cue environment (brown lines). For comparison, we also show the median regression line from the single cue environment analysis (Fig. 1h). **(d)**: Box plot for measured slopes in the single cue and multi-cue environments. The means of the slopes are significantly below zero in both the single cue and multi-cue setting (one-sided t-test, single cue $p < 10^{-3}$, multi-cue $p < 0.05$). Slopes in the single cue dataset are significantly more negative than in the multi-cue dataset (t-test, $p < 10^{-3}$). **(e)**: Example tuning curves in multi-cue dataset, split by the animal position in the arena (left - red, right - blue, compare Fig. 1i). **(f)**: Distribution of shifts in tuning curves when the animal is on the left/right side of the platform. Data aggregated over all HD neurons in all 16 sessions. For comparison, we also show the median peak shift of the single cue dataset analysis (orange dotted line, Fig. 1j), which is significantly more shifted than the multi-cue median peak shift (t-test, $p = 6.5 \cdot 10^{-3}$). **(g)**: Sketch to illustrate the 'in-view' (green) and 'out-of-view' (red) conditions. Vision cones filter the data for time periods where the cue is right in front (in-view) or behind (out-of-view) the animal. **(h)**: Resulting slope as an indicator of parallax strength in the in-view (green) and out-of-view (red) conditions for the single cue and multi-cue data. Significant differences are observed in the single cue dataset (t-test, $p < 10^{-3}$), whereas the slope remains close to zero in the multi-cue dataset in both conditions (t-test, $p = 0.169$).

Goodridge et al., 1998; Knierim et al., 1995; Zugaro, Berthoz, & Wiener, 2001; Zugaro, Tabuchi, et al., 2001; Bicanski & Burgess, 2016; Ocko et al., 2018; Page & Jeffery, 2018). Integrating these two signals naturally attenuates parallax, because anchorings to the visual cue occur at varying cue azimuths and therefore average over time. This averaging effect is expected to be even stronger with multiple cues (Gaussier et al., 2019), making complex correction mechanisms potentially unnecessary.

To test this quantitatively, we implemented a simple integrate-and-vision model (Fig. 4a), in which the HD estimate α_{iv} is a weighted sum of the AHV-integrated estimate α_{int} and the vision-based estimate α_{vis}:

$$\alpha_{iv}(t) = \sigma \cdot \alpha_{int}(t) + (1-\sigma) \cdot \alpha_{vis}(t) \cdot v_{cue}(t), \qquad (1)$$

where σ is the relative weighting of AHV integration and visual anchoring and $v_{cue}(t)$ is a binary variable indicating whether the visual cue is within the animal's field of vision. The inte-

grated estimate evolves as

$$\alpha_{\text{int}}(t) = \alpha_{\text{iv}}(t-1) + \Delta\alpha(t), \tag{2}$$

with the angular head displacement $\Delta\alpha(t)$ derived from the head tracking data. The "simulated mice" follow the same path and head direction as the real animals from the neural recordings. The model has two free parameters: σ and the angle of the field of vision. Both were estimated from cue-switching events in the single-cue dataset: the delay before reorientation allows us to estimate the field of vision, and the speed of reorientation allows us to estimate σ (Fig. 4e; Methods). Fitting exponential reorientation dynamics gave $\sigma = 0.997$ (Fig. 4f) and an effective field of vision angle of approximately 180° (Fig. 4g).

As expected, larger σ values reduce the influence of anchoring and therefore decrease the slope of the parallax relationship.

The simplified integrate-and-vision model is intended to demonstrate the principle of passive parallax attenuation, not to capture the full complexity of multisensory integration. I.e., in reality, the weighting between AHV integration and visual input likely varies with cue familiarity (Cheng et al., 2007; Julian et al., 2018) and the uncertainty (or variance) of α_{int} and α_{vis}, which could explain phenomena such as distance-dependent remapping (Zugaro, Berthoz, & Wiener, 2001). Because the variance of α_{int} in the neural system is unknown and AHV derived from the tracking system is very precise, we used a fixed σ and added a small amount of Gaussian noise to the AHV input (mean $0^\circ/\text{timestep}$, s.d. $0.2^\circ/\text{timestep}$) to obtain more realistic variability.

Repeating the linear regression parallax analysis on the modeled HD (treating α_{iv} as internal HD) confirmed that AHV integration is sufficient to reduce parallax relative to the geometric prediction of -1 for a purely vision-based system (Fig. 4b, black dashed vs. orange). The modeled slope w was sensitive to σ, which we cannot estimate with high precision, but the qualitative effect was robust. The model also reproduced the difference between cue-visible and cue-invisible conditions (Fig. 4c, green vs. red): slopes were steeper when the cue was visible.

We next extended the model to multiple cues. For each visible cue, we computed α_{vis} (Eq. 3) and took the circular mean across cues, using equal weighting for simplicity. Additional cues were assumed at the four corners of the room. In this multi-cue setting, the parallax bias almost vanished (Fig. 4d).

This simple integrate-and-vision model therefore demonstrates that the position-dependent parallax bias expected from geometry does arise in a single-cue environment, but is passively attenuated by AHV integration, and is almost eliminated when multiple cues are present. No active correction mechanism is required, consistent with the experimental findings above.

Discussion

Spatial navigation requires a stable allocentric sense of direction, yet sensory cues are perceived egocentrically. This necessitates a coordinate transformation whose underlying neural mechanism has been a long-standing question (Taube, 2007; Zhang, 1996). In this study, we provide evidence for a systematic parallax error in the head-direction (HD) signal of mice navigating an environment with only a single visual cue. This finding indicates that the HD system does not employ a complex, position-dependent correction mechanism, for instance, through place cell feedback, which would introduce a circular dependency, as place cells themselves require a stable HD signal (Bicanski & Burgess, 2016; McNaughton et al., 2006). Instead, our results support a model where the system relies on a simple, computationally efficient egocentric cue-anchoring strategy for the ego-to-allocentric transformation (Skaggs et al., 1994; Page & Jeffery, 2018). This process, while effective, inherently introduces a predictable, position-dependent bias when referencing a single, nearby landmark.

The artificial nature of a single-cue environment provides a unique window into the mechanism of this transformation. Understanding this mechanism is critical, as a stable allocentric HD signal is a fundamental prerequisite for downstream circuits in the hippocampal formation to build and maintain a coherent cognitive map (McNaughton et al., 2006; Tan et al., 2017).

A mechanism for anchoring the HD signal

The findings presented in this work suggest a specific model of how visual input is integrated in the HD network. A major challenge of this integration is the fact that visual observations are inherently egocentric, but the head direction is an allocentric signal. Therefore, the HD network needs to perform an egocentric-to-allocentric coordinate transform. This coordinate transform is widely believed to involve the retrosplenial cortex (RSC) and PoSub Goodridge & Taube (1997); Clark et al. (2010). RSC contains cells encoding the egocentric angle to specific environmental features and HD cells driven primarily by visual landmarks (Alexander et al., 2020; Jacob et al., 2017). PoSub thus receives input both from the visual HD pathway through the RSC, as well as from the movement-integrating pathway through the antero-dorsal thalamic nucleus (ADN) (Fig. 5). For a detailed description of the movement integration pathway and how to model it, see Bicanski & Burgess (2016).

An open question in the literature so far is the exact mechanism that allows the egocentric-to-allocentric transformation in the HD network. Given the experimental results provided in this study, we propose the following solution: Bearing cells in RSC map onto an HD ring attractor in PoSub with a fixed offset. This fixed offset is what determines the anchoring angle in the previous analysis. Specific bearing cell ring attractors may be activated by visual cues, whose identity and egocentric position is provided by the visual system (Fig. 5).

Any single bearing cell ring attractor is subject to the parallax effect. Therefore, in a highly restricted setting of only one singular cue in the environment, this parallax error is also present in the postsubiculum. However, in practice, we always observe multiple bearing cell ring attractors being active for

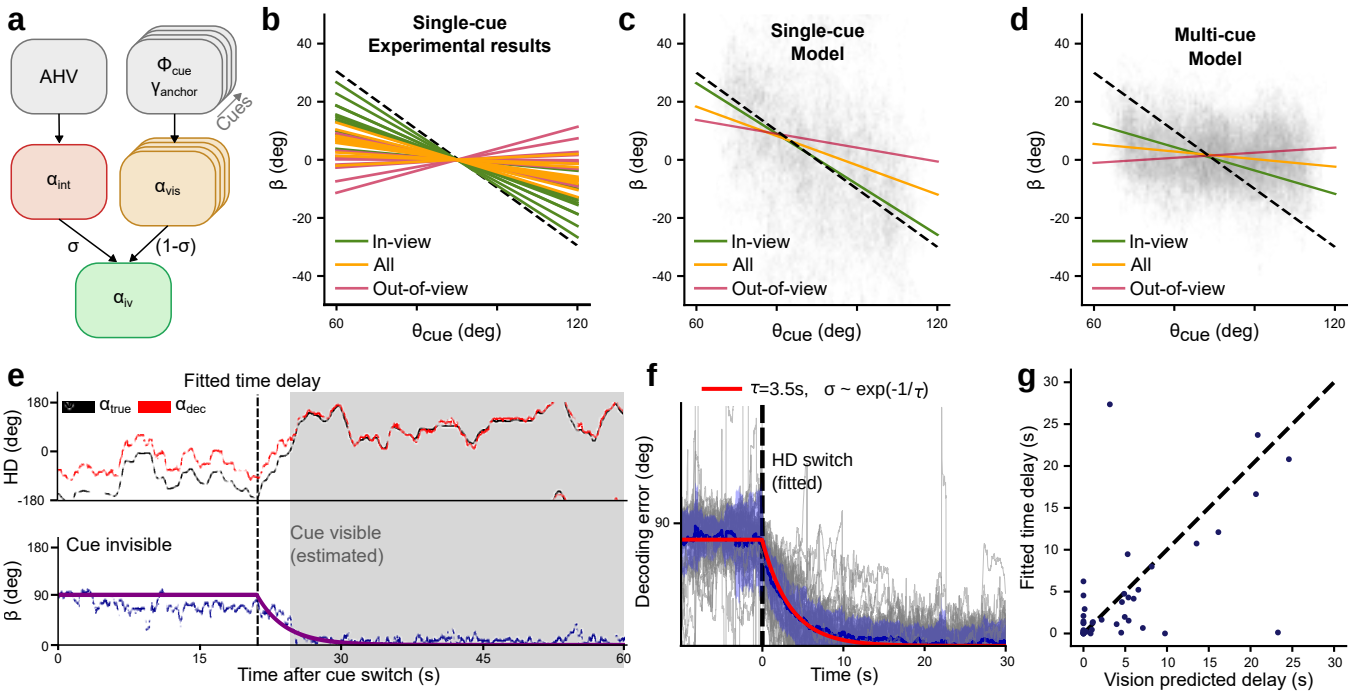

Figure 4: **Simulations confirm that AHV and the use of multiple cues neutralize the measured parallax effect.** (**a**): Visualization of the simulated HD model, as described in Eqs. (1, 2). (**b**): Single-cue experiment experimentally determined linear regression slopes as a reference for the modeling results in panels (c) and (d). Slopes for complete sessions are shown in orange, filtered for the in-view condition in green and out-of-view condition in red. (**c**): Fitted slopes from simulated head direction using a single cue. A negative slope with a magnitude below 1 (black dashed line) is observed in all three conditions. The slope is steeper in periods when the cue is in view (green) and less steep when the cue is out of view (brown), matching our experimental observations. (**d**): Parallax analysis on the simulated data with multiple cues (cue card and the four corners of the square environment). Overall, parallax is drastically attenuated compared to (b). (**e**): Example beginning of a trial with fitted HD switching onset and exponential decay fit shown in the bottom panel. Gray background color indicates when the cue is in-view, according to a 180° field of vision. (**f**): All HD reorientation events aligned on the fitted time delay. The resulting mean decay shows a time constant $\tau = 3.5s$, which we use to determine the weighting between visual and integrated HD estimates. (**g**): Distribution of fitted time delays and time delays predicted by a 180° field of vision.

multiple cues. The postsubiculum at this point acts as the average approximation of all visual estimates together with the movement integrated input from the ADN (akin to the simulated α_{iv} above).

The weighting between the different bearing cell rings and the ADN input could be established by the gain of each population (effectively the height of the activity bump in each ring attractor) (Ajabi et al., 2023). The gain of each ring attractor may be determined by how fast the activity bump is moving along the attractor manifold, where immobile activity bumps are weighted higher than fast-moving ones. Such a weighting mechanism would result in close-by visual cues to influence the PoSub HD less, as their azimuth changes faster than those of more distant cues. This weighting would also give more weight to stationary objects rather than moving ones. It would finally also weigh movement-integrated estimates vs. visual estimates, relying more strongly on vision when the head is moved quickly and the movement integration is more prone to inaccurate HD estimates.

Finally, in our conceptual model, as already suggested in previous studies, PoSub sends its combined HD signal back to RSC and ADN/LMN as a correction mechanism. Additionally, PoSub propagates the combined HD estimate forward to the hippocampal formation for subsequent position estimation.

This direct mapping strategy of self-motion information and bearing information of multiple objects onto one ring attractor is fast and computationally efficient, as it does not require explicit positional information to compute an HD estimate. Such efficiency is a critical advantage for both biological and artificial navigation systems, where energy and processing resources are constrained (Renner et al., 2022; Arleo & Gerstner, 2000). This work highlights a fundamental trade-off between computational simplicity and absolute positional accuracy in neural coding.

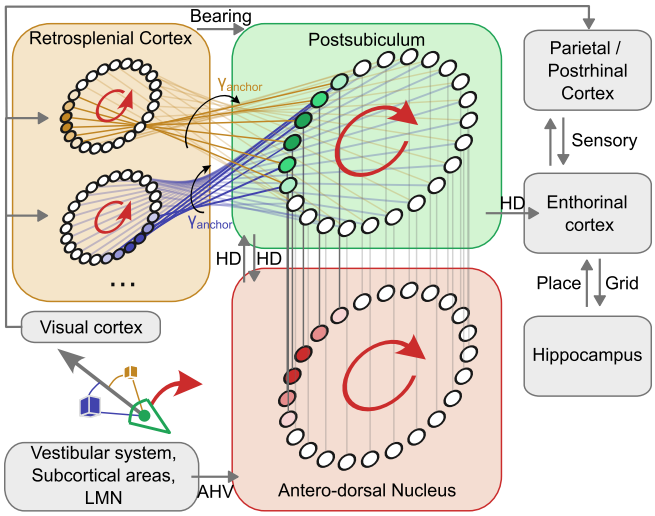

Figure 5: **Conceptual model of the HD formation from combined AHV integration and visual inputs**. Based on visual inputs and inertial movement measurements (bottom left), visual cortices and subcortical areas transmit information along different pathways. The visual information is mapped to bearing cell rings in retrosplenial cortex (RSC). These, in turn, have a fixed anchoring angle to map onto the head direction cells in the postsubiculum (PoSub). The inertial measurements in turn are projected through LMN to the Antero-dorsal Nucleus (AdN) (see Bicanski & Burgess (2016) for a detailed description of this mechanism). PoSub acts as a central integrator in this model, combining the visual and integrated HD states and relaying them back to RSC and AdN and projecting them forward to the entorhinal cortex for subsequent position-estimation in the hippocampal formation.

The anchoring angle as a link between egocentric and allocentric frames.

The anchoring angle, γ_{anchor}, provides a simple geometric description of how egocentric visual cues become aligned with the allocentric HD representation. It effectively marks the phase offset between the retrosplenial populations encoding the egocentric cue bearing and the postsubicular HD ring that represents allocentric head direction (Alexander et al., 2020; Bicanski & Burgess, 2020). Once established, this offset acts as a stable "reference phase" between sensory and internal frames of reference.

Here, we have shown that the parallax effect can be used as a measurement tool to estimate this important property of the egocentric to allocentric mapping.

Conceptually, γ_{anchor} can be viewed as a memory of the cue azimuth at which cue control was first acquired. When the same landmark reappears, the HD system tends to pull the internal compass back toward this learned offset. This explains why, after experimentally introduced cue rotations, the system realigns instantly when the cue is recognized as familiar but fails to do so when it is perceived as novel.

Why parallax has remained hidden

The absence of previous reports on the parallax effect warrants explanation. Our findings suggest two primary reasons. First, the HD system continuously integrates AHV, which inherently smooths the visual error over time as the animal moves through the environment (McNaughton et al., 1991; Taube, 2007). Our data directly support this, showing that the measured parallax error was significantly attenuated when the cue was not in the animal's direct field of view. Second, and more importantly, naturalistic environments are rich with visual and other directional sensory cues. Our analysis of recordings from a multi-cue setting revealed a practical elimination of the parallax error. This strongly supports the hypothesis that the HD system averages heading estimates derived from multiple landmarks to form a unified, robust signal (Gaussier et al., 2019; Goodridge et al., 1998). The individual parallax errors associated with each cue, having different spatial dependencies, effectively cancel each other out. Most experimental paradigms, even those with a primary cue card, likely provide sufficient secondary cues (e.g., arena corners, arena geometry, shadows, equipment, odors, sounds) to enable this averaging, thus masking the parallax from any single cue.

Parallax-bias is a system-wide phenomenon

The impact of parallax is not limited to a subset of specialized cells but is a system-wide phenomenon. Our single-neuron analysis revealed that the preferred firing directions of individual HD neurons shift systematically with the animal's position relative to the cue. This confirms that the entire HD attractor network is biased by the visual input in the single-cue context, rather than the effect being an artifact of a few bearing-like cells.

Conclusion

In conclusion, our study demonstrates that the mammalian HD system is subject to parallax error when constrained to a single visual landmark. This finding strongly supports a model of simple egocentric cue-anchoring, a computationally efficient strategy for ego-to-allocentric transformation. The apparent vulnerability to error is robustly overcome in natural settings through the parallel integration of self-motion cues and the averaging of information from multiple environmental landmarks. This work clarifies a key mechanism of spatial cognition and highlights an elegant solution for generating a stable allocentric signal, offering insights that can inform the development of more robust and efficient bio-inspired navigation systems. Further research should build on these findings to investigate whether parallax error propagates to other nodes of the navigation circuit, such as the medial entorhinal cortex, which could further elucidate how the brain ensures a stable directional reference for navigation.

Methods

Single Cue experiment

We analyzed publicly available neural recordings from the postsubiculum (PoSub) of six sessions of six mice during the

"Cue Rotation Task" reported in (Duszkiewicz et al., 2024). We were additionally provided with five previously unpublished sessions of the same experimental setup, so overall, we report on 11 sessions of 10 mice. Each session includes the tracked head position and direction, as well as the recorded spike trains. The mice freely explored a 30 cm diameter elevated circular platform within a 90 cm darkened square enclosure (Fig. 1A) for approximately 75 minutes per session. Visual cues, consisting of dim LED strips forming a "V" or "X" shape (approximately 10 cm wide), were positioned at the center of each wall and treated as point sources for analysis. Surgical procedures, electrophysiological recording details, spike sorting and neuron classification procedures, as well as the exact experimental protocol, are described in (Duszkiewicz et al., 2024). Each session began with a stable cue presentation (habituation period, 14-21 minutes). Subsequently, this initial cue was turned off, and a cue on an adjacent wall was activated. The experimental protocol comprised 16 200-second trials, with the active cue alternating between the two LEDs after each trial. Only one cue was active at any time. In the additionally provided 5 datasets, the mice's HD neurons did not reorient during the cue rotation, but kept their orientation throughout the sessions. Unless otherwise specified, we reoriented the position data for these cases in each trial such that the cue was effectively always positioned at the north wall (Fig. 1c).

Multi-Cue experiment

We also analyzed publicly available square open field recordings of 16 mice from the same publication (Duszkiewicz et al., 2024). Neural activity was again recorded from PoSub, and the animal's position and head direction were tracked. The environment consisted of a 90 cm x 90 cm square box with a single cue card on one of the walls to serve as a cue. A key difference between this experimental setup and the previous "single-cue" environment is the lighting conditions. The environment was illuminated, allowing the animal to also see the enclosure and any features within the environment clearly. Therefore, while only a single intentional cue in the form of a cue card has been added to the environment, the animals may to use additional features as cues to anchor their HD estimates. Surgical procedures, electrophysiological recording details, and the exact experimental protocol are again described in (Duszkiewicz et al., 2024).

Data Exclusion

In all datasets, we excluded periods where the mice exhibited prolonged immobility, as these periods led to less activity and an unreliable decoded HD signal. We achieved this by estimating the animal's speed from the tracked position. We then smoothed this position signal (square kernel, 0.5 s width) and rejected time periods in which the absolute value of the smoothed speed was below $2\frac{cm}{s}$. We additionally excluded the time periods that were used to compute the tuning curves for each neuron from all further analysis. For the tuning curve estimation, we used the first 10 min of each recording. In the single cue experiment sessions, we also estimated the time period of HD reorientation at the beginning of the trial and excluded these time windows from the parallax analysis. In the sessions without reorientation, we only considered the trials of the original cue orientation.

HD Decoding

As Duszkiewicz et al. (2024), we performed Bayesian decoding (Zhang et al., 1998) on the head direction cells (cell labeling adopted from the dataset). Tuning curves for all head direction neurons were computed using the first 10 minutes of the recording (part of the habituation period in the single cue experiment and just the first 10 min of recording in the square arena dataset). This period was excluded from subsequent analysis. The Bayesian decoder treats these tuning curves as conditional probability distributions of head direction given a neuron's firing. For each time bin of 10 ms, the likelihood distribution of the head direction was calculated by multiplying the tuning curves of all spiking neurons within that bin. The prior is the head direction distribution of the preceding time bin and discourages large jumps between consecutive estimates. The head direction estimate for each time bin was then obtained by identifying the peak of the resulting posterior. Notably, the number of HD neurons per dataset varied between all sessions ($25-117$ recorded HD units, mean: 69 ± 23 units). This led to a difference in decoding quality ($RMSE: 0.75^\circ - 1.6^\circ$, mean RMSE: $1.1^\circ \pm 0.2^\circ$). RMSE and number of neurons for all sessions can be found in Suppl. Fig. 13.

Cue visibility conditions

In Sec. The parallax effect is dependent on cue visibility, we test whether the visibility of the cue has an influence on the amount of parallax detected in the experimental data. We differentiate an "in-view" and "out-of-view" condition and perform the parallax analysis on both separately. For the "in-view" condition, we only consider time periods in which the egocentric viewing angle $\phi_{\text{cue}}(t)$ is within $\pm 45^\circ$, meaning that the cue is within a 90° vision cone of the animal. The "out-of-view condition" is likewise defined as time periods in which $\phi_{\text{cue}}(t)$ is within $180^\circ \pm 45^\circ$. We use these rather small cones of vision as a conservative measure to ensure that the animal is facing either directly towards or away from the cue. The data rejection criteria are also applied to these two subsets of the data before any further analysis.

Linear regression and bootstrapping

In a simple cue anchoring model, there exists a fixed mapping between the egocentric viewing angle of the cue ϕ_{cue} and the vision based HD estimate α_{vis} that is defined by the anchoring angle γ_{anchor}:

$$\alpha_{\text{vis}}(t) = \gamma_{\text{anchor}} - \phi_{\text{cue}}(t). \tag{3}$$

The egocentric viewing angle ϕ_{cue} is defined as the difference between the true head direction α_{true} and the allocentric cue angle θ_{cue} (that is, the angle of the vector pointing from

the animal to the cue):

$$\phi_{\text{cue}}(t) = \theta_{\text{cue}}(t) - \alpha_{\text{true}}(t). \tag{4}$$

Substituting Eq. 4 in Eq. 3, we obtain a linear relationship (up to the angular periodicity) between the decoding error β_{vis} and the position dependent allocentric cue angle θ_{cue} (Fig.1c,d.):

$$\begin{aligned}\beta_{\text{vis}}(t) &= \alpha_{\text{vis}}(t) - \alpha_{\text{true}}(t) \\ &= \gamma_{\text{anchor}} - \theta_{\text{cue}}(t).\end{aligned} \tag{5}$$

Equivalently, we can view the allocentric cue angle θ_{cue} as the angle of the vector from the subject to the cue. In this view, the linear relationship in Eq. 5 tells us that we expect a systematic, linear relationship between the HD bias and the position of the subject in the simple cue anchoring model. If the subject were only guided by visual input, we would expect that linear relationship to have a slope of -1 and an offset given by the fixed anchoring angle.

To test whether this HD bias relation is also detectable in experimental data, we used the measured HD bias β_{dec} of the each mouse as the angular differences between the tracked and internal HD. We also computed the allocentric cue angle $\theta_{\text{cue}}(t)$ from the animals' tracked position. We then performed a bootstrapped linear regression:

$$\beta_{\text{dec}}(t) = w \cdot \theta_{\text{cue}} + b + \varepsilon(t), \tag{6}$$

where the slope w and intercept b are fitted parameters minimizing the squared error of the linear fit to the observed data points. ε is the residual.

Eq. 6 corresponds to Eq 5, where the slope is $w = -1$ and the intercept $b = -w \cdot \gamma_{\text{anchor}}$. Note that the linear regression fits the y-intercept, while the anchoring angle is the x-intercept.

We use a linear regression between the decoding error β and the allocentric cue angle θ_{cue} to measure the amount of parallax and determine the anchoring angle. The linear regression is implemented as a least square optimizer using the "SciPy" package in Python. To account for autocorrelations in the time series data, we use stationary block bootstrapping (Politis & Romano, 1994) with an average block length of 2.5 s and n=1000 iterations to estimate the slopes, intercepts, and standard errors of w and b, as well as the p-values for the respective fits.

We apply the same procedure to obtain slopes and offsets for each entire session (after applying the rejection criteria described above), and for subsets of the session where the animal is looking directly towards or away from the cue to obtain the detected parallax in the "all data", "in-view", and "out-of-view" conditions.

Computing the anchoring angle

The anchoring angle γ_{anchor} is calculated from the results of the bootstrapped linear regression as

$$\gamma_{\text{anchor}} = -b/w. \tag{7}$$

Uncertainties were propagated using standard error propagation:

$$\sigma_\gamma = |\gamma_{\text{anchor}}| \times \sqrt{\left(\frac{\sigma_b}{b}\right)^2 + \left(\frac{\sigma_w}{w}\right)^2}, \tag{8}$$

where σ_b and σ_w are the bootstrapped standard errors of the intercept and slope, respectively.

We assume that each cue and each animal has a distinct anchoring angle. Therefore, the fit was performed separately for each session (Fig. 3a). We observed fitted slopes w significantly below 0 for ten out of eleven recording sessions (weighted mean slope $\overline{w} = -0.23 \pm 0.008$), meaning that the parallax error can be observed in all but one sessions (bootstrapped t-test, p-values < 0.05, Suppl. Tab. 3). However, the maximal negative measured slope was -0.43, indicating a lower position dependence of the decoding error than predicted by a pure vision model (where we would expect a slope of -1). Furthermore, the relatively low R^2 values (range: $0.001 - 0.127$, see Suppl. Tab. 3) suggest that additional factors influence HD decoding errors. One essential and well-known additional factor is AHV integration, which we examine in the next section.

Determining field of vision and weighting from cue switches

The integrate-and-vision model (Eq. 1) is dependent on a weighting factor σ and the field of vision. Both parameters can be estimated by analyzing the cue-switching periods of the single cue experiment recordings. At the beginning of each trial of these sessions, we see a reorientation event, where the decoded HD takes some time to adjust to the new cue's position. We estimate this period by fitting a delayed exponential decay to the decoding error in these periods (Fig. 4d, purple). The time constant of the exponential decay τ tells us how fast the visual input changes the current HD estimate and is directly related to the weighting of the integrated and the visual input by $\sigma = e^{-\frac{1}{tau \cdot s}}$, where s is the sampling rate. As we find the mean time constant is $\tau = 3.5\ s$ (Fig. 4e), we obtain a weighting factor $\sigma = 0.997$.

Furthermore, we hypothesize that the delay before the onset of the exponential decay might be due to the effective field of vision of the animal, that is, the viewing angle range in which the animals are using landmarks for the visual anchoring. Based on the fitted anchoring angle, we observe that an effective field of vision of 180° best fits the fitted time delays (Fig. 4d,f).

Software

Code was written in Python 3.12 using numpy, matplotlib, and scipy for analysis and visualization. Fits were performed using the scipy.stats.linregress function, bootstrapping using the arch package and MSE minimization for σ using the optuna package.

Data availability

For this work, the data from Duszkiewicz et al. (2024) and additional recordings in the same setting

were used. The published data can be found here: 10.6084/m9.figshare.24921252. The additional data will be made available at the time of publication of this paper.

Code availability

The code for the analysis and model will be made available at the time of publication of this paper.

Acknowledgements

We thank Johannes Leugering, Paxon Frady and Viet Anh Khoa Tran for their feedback. Generative AI was used, with care, to optimize and document code and to support writing. This research is funded by VolkswagenStiftung [CLAM 9C854].

Author contributions

A.R. and S.K. designed the study and the the computational models. A.J.D. collected the experimental data. S.K. performed the data analyses and implemented the models. A.R., E.N., and F.T.S. supervised the project. A.R., S.K., A.J.D., E.N., and F.T.S. wrote the manuscript.

References

Ajabi, Z., Keinath, A. T., Wei, X.-X., & Brandon, M. P. (2023, March). Population dynamics of head-direction neurons during drift and reorientation. *Nature*, *615*(7954), 892–899. doi: 10.1038/s41586-023-05813-2

Alexander, A. S., Carstensen, L. C., Hinman, J. R., Raudies, F., Chapman, G. W., & Hasselmo, M. E. (2020). Egocentric boundary vector tuning of the retrosplenial cortex. *Science advances*, *6*(8), eaaz2322.

Arleo, A., & Gerstner, W. (2000). Modeling rodent head-direction cells and place cells for spatial learning in biomimetic robotics. *From Animals to Animats*, *6*, 236–245.

Bassett, J. P., & Taube, J. S. (2001, August). Neural Correlates for Angular Head Velocity in the Rat Dorsal Tegmental Nucleus. *Journal of Neuroscience*, *21*(15), 5740–5751. doi: 10.1523/JNEUROSCI.21-15-05740.2001

Bicanski, A., & Burgess, N. (2016). Environmental anchoring of head direction in a computational model of retrosplenial cortex. *Journal of Neuroscience*, *36*(46), 11601–11618.

Bicanski, A., & Burgess, N. (2020, September). Neuronal vector coding in spatial cognition. *Nature Reviews Neuroscience*, *21*(9), 453–470. doi: 10.1038/s41583-020-0336-9

Blair, H. T., & Sharp, P. E. (1996). Visual and vestibular influences on head-direction cells in the anterior thalamus of the rat. *Behavioral neuroscience*, *110*(4), 643.

Boucheny, C., Brunel, N., & Arleo, A. (2005, March). A Continuous Attractor Network Model Without Recurrent Excitation: Maintenance and Integration in the Head Direction Cell System. *Journal of Computational Neuroscience*, *18*(2), 205–227. doi: 10.1007/s10827-005-6559-y

Burak, Y., & Fiete, I. R. (2009, February). Accurate Path Integration in Continuous Attractor Network Models of Grid Cells. *PLoS Computational Biology*, *5*(2), e1000291. doi: 10.1371/journal.pcbi.1000291

Cheng, K., Shettleworth, S. J., Huttenlocher, J., & Rieser, J. J. (2007). Bayesian integration of spatial information. *Psychological bulletin*, *133*(4), 625.

Clark, B. J., Bassett, J. P., Wang, S. S., & Taube, J. S. (2010). Impaired head direction cell representation in the anterodorsal thalamus after lesions of the retrosplenial cortex. *Journal of Neuroscience*, *30*(15), 5289–5302.

Duszkiewicz, A. J., Fricker, D., Burgalossi, A., & Peyrache, A. (2025). The postsubiculum as a head-direction cortex. *Trends in Neurosciences*.

Duszkiewicz, A. J., Orhan, P., Skromne Carrasco, S., Brown, E. H., Owczarek, E., Vite, G. R., ... Peyrache, A. (2024, April). Local origin of excitatory–inhibitory tuning equivalence in a cortical network. *Nature Neuroscience*, *27*(4), 782–792. doi: 10.1038/s41593-024-01588-5

Gaussier, P., Banquet, J. P., Cuperlier, N., Quoy, M., Aubin, L., Jacob, P.-Y., ... Poucet, B. (2019). Merging information in the entorhinal cortex: what can we learn from robotics experiments and modeling? *Journal of Experimental Biology*, *222*(Suppl_1), jeb186932.

Goodridge, J. P., Dudchenko, P. A., Worboys, K. A., Golob, E. J., & Taube, J. S. (1998). Cue control and head direction cells. *Behavioral neuroscience*, *112*(4), 749.

Goodridge, J. P., & Taube, J. S. (1997). Interaction between the postsubiculum and anterior thalamus in the generation of head direction cell activity. *Journal of Neuroscience*, *17*(23), 9315–9330. doi: 10.1523/JNEUROSCI.17-23-09315.1997

Hahnloser, R. H. R. (2003, September). Emergence of neural integration in the head-direction system by visual supervision. *Neuroscience*, *120*(3), 877–891. doi: 10.1016/S0306-4522(03)00201-X

Harland, B., Grieves, R. M., Bett, D., Stentiford, R., Wood, E. R., & Dudchenko, P. A. (2017, September). Lesions of the Head Direction Cell System Increase Hippocampal Place Field Repetition. *Current Biology*, *27*(17), 2706-2712.e2. doi: 10.1016/j.cub.2017.07.071

Jacob, P.-Y., Casali, G., Spieser, L., Page, H., Overington, D., & Jeffery, K. (2017, February). An independent, landmark-dominated head-direction signal in dysgranular retrosplenial cortex. *Nature Neuroscience*, *20*(2), 173–175. doi: 10.1038/nn.4465

Julian, J. B., Keinath, A. T., Marchette, S. A., & Epstein, R. A. (2018). The neurocognitive basis of spatial reorientation. *Current Biology*, *28*(17), R1059–R1073.

Kim, M., & Maguire, E. A. (2019). Encoding of 3D head direction information in the human brain. *Hippocampus*, *29*(7), 619–629. doi: 10.1002/hipo.23060

Knierim, J. J., Kudrimoti, H. S., & McNaughton, B. L. (1995). Place cells, head direction cells, and the learning of landmark stability. *Journal of Neuroscience*, *15*(3), 1648–1659.

McNaughton, B. L., Battaglia, F. P., Jensen, O., Moser, E. I., & Moser, M.-B. (2006, August). Path integration and the neural basis of the 'cognitive map'. *Nature Reviews Neuroscience*, *7*(8), 663–678. doi: 10.1038/nrn1932

McNaughton, B. L., Chen, L., & Markus, E. (1991). "dead reckoning," landmark learning, and the sense of direction: a neurophysiological and computational hypothesis. *Journal of Cognitive Neuroscience*, *3*(2), 190–202.

Mizumori, S., & Williams, J. (1993, September). Directionally selective mnemonic properties of neurons in the lateral dorsal nucleus of the thalamus of rats. *The Journal of Neuroscience*, *13*(9), 4015–4028. doi: 10.1523/JNEUROSCI.13-09-04015.1993

Ocko, S. A., Hardcastle, K., Giocomo, L. M., & Ganguli, S. (2018). Emergent elasticity in the neural code for space. *Proceedings of the National Academy of Sciences*, *115*(50), E11798–E11806.

Page, H. J., & Jeffery, K. J. (2018). Landmark-based updating of the head direction system by retrosplenial cortex: a computational model. *Frontiers in Cellular Neuroscience*, *12*, 191.

Petrucco, L., Lavian, H., Wu, Y. K., Svara, F., Štih, V., & Portugues, R. (2023, May). Neural dynamics and architecture of the heading direction circuit in zebrafish. *Nature Neuroscience*, *26*(5), 765–773. doi: 10.1038/s41593-023-01308-5

Politis, D. N., & Romano, J. P. (1994). The stationary bootstrap. *Journal of the American Statistical Association*, *89*(428), 1303–1313. doi: 10.1080/01621459.1994.10476870

Rank, J. (1984). Head-direction cells in the deep layers of dorsal presubiculum of freely moving rats. In *Soc. neuroscience abstr.* (Vol. 10, p. 599).

Renner, A., Supic, L., Danielescu, A., Indiveri, G., Frady, E. P., Sommer, F. T., & Sandamirskaya, Y. (2022). Visual odometry with neuromorphic resonator networks. *arXiv preprint arXiv:2209.02000*.

Sharp, P. E., Tinkelman, A., & Cho, J. (2001). Angular velocity and head direction signals recorded from the dorsal tegmental nucleus of gudden in the rat: Implications for path integration in the head direction cell circuit. *Behavioral Neuroscience*, *115*(3), 571–588. doi: 10.1037/0735-7044.115.3.571

Skaggs, W., Knierim, J., Kudrimoti, H., & McNaughton, B. (1994). A model of the neural basis of the rat's sense of direction. *Advances in neural information processing systems*, *7*.

Tan, H. M., Wills, T. J., & Cacucci, F. (2017). The development of spatial and memory circuits in the rat. *WIREs Cognitive Science*, *8*(3), e1424. doi: 10.1002/wcs.1424

Taube. (1995). Head direction cells recorded in the anterior thalamic nuclei of freely moving rats. *Journal of Neuroscience*, *15*(1), 70–86.

Taube. (2007, July). The Head Direction Signal: Origins and Sensory-Motor Integration. *Annual Review of Neuroscience*, *30*(Volume 30, 2007), 181–207. doi: 10.1146/annurev.neuro.29.051605.112854

Taube, Muller, R., & Ranck, J. (1990b, February). Head-direction cells recorded from the postsubiculum in freely moving rats. II. Effects of environmental manipulations. *The Journal of Neuroscience*, *10*(2), 436–447. doi: 10.1523/JNEUROSCI.10-02-00436.1990

Taube, Muller, R. U., & Ranck, J. B. (1990a, February). Head-direction cells recorded from the postsubiculum in freely moving rats. I. Description and quantitative analysis. *The Journal of Neuroscience: The Official Journal of the Society for Neuroscience*, *10*(2), 420–435. doi: 10.1523/JNEUROSCI.10-02-00420.1990

van Beest, E. H., Mukherjee, S., Kirchberger, L., Schnabel, U. H., van der Togt, C., Teeuwen, R. R., ... others (2021). Mouse visual cortex contains a region of enhanced spatial resolution. *Nature communications*, *12*(1), 4029.

Winter, S. S., Clark, B. J., & Taube, J. S. (2015). Disruption of the head direction cell network impairs the parahippocampal grid cell signal. *Science*, *347*(6224), 870–874.

Zhang, K. (1996). Representation of spatial orientation by the intrinsic dynamics of the head-direction cell ensemble: a theory. *Journal of Neuroscience*, *16*(6), 2112–2126.

Zhang, K., Ginzburg, I., McNaughton, B. L., & Sejnowski, T. J. (1998). Interpreting neuronal population activity by reconstruction: unified framework with application to hippocampal place cells. *Journal of neurophysiology*, *79*(2), 1017–1044.

Zugaro, M. B., Arleo, A., Berthoz, A., & Wiener, S. I. (2003, April). Rapid Spatial Reorientation and Head Direction Cells. *Journal of Neuroscience*, *23*(8), 3478–3482. doi: 10.1523/JNEUROSCI.23-08-03478.2003

Zugaro, M. B., Berthoz, A., & Wiener, S. I. (2001, July). Background, But Not Foreground, Spatial Cues Are Taken as References for Head Direction Responses by Rat Anterodorsal Thalamus Neurons. *The Journal of Neuroscience*, *21*(14), RC154-RC154. doi: 10.1523/JNEUROSCI.21-14-j0001.2001

Zugaro, M. B., Tabuchi, E., Fouquier, C., Berthoz, A., & Wiener, S. I. (2001). Active locomotion increases peak firing rates of anterodorsal thalamic head direction cells. *Journal of neurophysiology*, *86*(2), 692–702.

Supplementary Material

Analysis of tuning curves from only the center of the environment

The analysis presented in the main part of this paper relies on the computed tuning curves from the neural activity. To ensure that there is no bias in the tuning curve that would explain the detected parallax, we repeated the analysis, but computed the tuning curves only from time periods where the animal was in the center of the environment, where we expect the parallax to be minimal and therefore not influence the tuning curves. We found that the parallax effect remains detectable in this analysis and noted no qualitative differences from the analysis presented in the main text. As can be seen in Fig. 6, we obtain the same

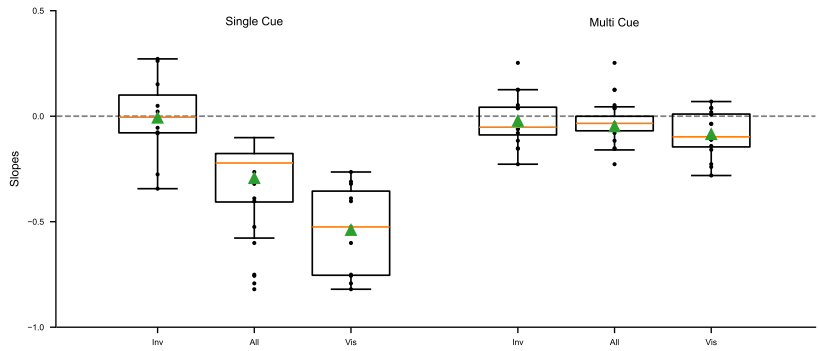

Figure 6: **Results of parallax analysis using tuning curves from the center of the environment.** The distribution of measured slopes from the linear regression is presented in the two experimental setups, "Single cue" and "multi-cue". The three conditions "in-view", "all data", and "out-of-view" (from left to right) are defined as in the main text (see Figs. 1h inset and 3d,h)

.

detectable, but reduced parallax in the single cue setting and a strongly reduced parallax effect in the multi-cue setting. The cue visibility pattern also remains, i.e., we find a stronger parallax effect in the subset of time in each session where the animal is facing towards the cue and a lower amount of parallax in time periods where the animal is facing away from the cue.

Significance testing results

Table 1: Statistical comparison of decoding errors between left and right arena positions across all recording sessions in the single cue dataset. All p-values remain significant after Bonferroni correction for multiple comparisons ($\alpha = 0.0045$). Effect sizes: negligible ($|d| < 0.2$), small ($0.2 \leq |d| < 0.5$), medium ($0.5 \leq |d| < 0.8$), large ($|d| \geq 0.8$).

Session	Sample Size		Left Side		Right Side		Test	Statistics			Effect	Effect
	Left	Right	Mean (°)	SD (°)	Mean (°)	SD (°)	Type	t-stat	df	p-value	Cohen's d	Size
A3702-191128	69,417	74,450	3.011	14.640	−4.783	12.561	Welch's	108.00	137159.5	< 0.001	0.57	Medium
A3706-200315	43,598	24,753	−3.988	10.257	−16.873	12.570	Welch's	137.39	43476.6	< 0.001	1.16	Large
A3716-201015	54,813	57,448	4.295	17.628	2.250	14.995	Welch's	20.89	107660.9	< 0.001	0.13	Negligible
A3707-200318	82,481	57,669	4.122	13.801	−3.105	12.571	Welch's	101.70	130845.0	< 0.001	0.54	Medium
A3717-201022	17,240	81,368	1.737	19.206	−2.230	20.188	Welch's	24.41	25953.3	< 0.001	0.20	Negligible
A3730-210324	38,263	35,356	0.457	10.843	−3.095	10.164	Welch's	45.88	73601.8	< 0.001	0.34	Small
A3701-191120	58,524	135,020	2.005	16.143	−0.211	12.299	Welch's	29.68	89228.8	< 0.001	0.16	Negligible
A3705-200307	52,669	60,660	−4.433	12.816	−10.625	13.461	Student's	78.97	113327.0	< 0.001	0.47	Small
A3711-200815	23,141	15,398	3.871	22.702	−5.200	28.219	Student's	34.81	38537.0	< 0.001	0.36	Small
A3711-200810	37,485	45,425	2.351	15.850	−2.117	14.414	Welch's	42.08	76647.8	< 0.001	0.30	Small
A3712-200903b	68,480	35,945	−8.725	17.593	−6.250	14.205	Welch's	−24.58	87385.6	< 0.001	−0.15	Negligible

* Test type determined by Levene's test for equality of variances

Table 2: Statistical comparison of slope distributions across viewing conditions and datasets. Slopes represent the relationship between landmark angle and decoding error. Significance levels: *** $p < 0.001$, ** $p < 0.01$, * $p < 0.05$, ns = not significant.

Dataset	**Condition 1**	**Condition 2**	**Test**	**p-value**	**Significance**
Single Cue					
	In-view	Out-of-view	t-test	< 0.001	***
	All	Out-of-view	t-test	0.010	*
	In-view	All	t-test	0.001	**
multi-cue					
	In-view	Out-of-view	t-test	0.169	ns
	All	Out-of-view	t-test	0.497	ns
	In-view	All	t-test	0.327	ns
Between Datasets					
	Single Cue, Out-of-view	Multi-Cue, Out-of-view	t-test	0.827	ns
	Single Cue, All Data	Multi-Cue, All Data	t-test	< 0.001	***
	Single Cue, In-View	Multi-Cue, In-View	t-test	< 0.001	***

All comparisons used independent samples t-tests after Shapiro-Wilk normality testing

Table 3: Parallax Analysis Results - Single Cue. Anchoring angles with errors $> 180^\circ$ are not reported.

Session	Condition	w	SD	p-value	R^2	γ_{anchor} (deg)	Significance
A3702-191128	Out-of-view	-0.030	0.030	0.309	0.001	-56.5 ± 105.9	ns
	All data	-0.346	0.020	< 0.001	0.084	89.3 ± 7.5	***
	In-view	-0.888	0.061	< 0.001	0.279	95.8 ± 9.3	***
A3706-200315	Out-of-view	-0.233	0.067	< 0.001	0.026	60.2 ± 28.4	***
	All data	-0.428	0.029	< 0.001	0.127	66.3 ± 7.3	***
	In-view	-0.758	0.089	< 0.001	0.174	79.0 ± 14.8	***
A3716-201015	Out-of-view	0.091	0.066	0.167	0.001	4.7 ± 64.7	ns
	All data	-0.197	0.025	< 0.001	0.009	112.7 ± 18.5	***
	In-view	-0.467	0.052	< 0.001	0.078	96.2 ± 15.0	***
A3707-200318	Out-of-view	-0.308	0.048	< 0.001	0.069	81.2 ± 20.4	***
	All data	-0.275	0.018	< 0.001	0.072	87.1 ± 8.3	***
	In-view	-0.127	0.078	0.103	0.008	90.5 ± 71.9	ns
A3717-201022	Out-of-view	-0.006	0.085	0.944	0.000	-	ns
	All data	-0.087	0.044	0.045	0.001	66.3 ± 59.0	*
	In-view	-0.438	0.080	< 0.001	0.042	93.1 ± 25.0	***
A3730-210324	Out-of-view	-0.106	0.041	0.010	0.004	47.0 ± 40.8	**
	All data	-0.222	0.019	< 0.001	0.032	78.1 ± 10.2	***
	In-view	-0.297	0.055	< 0.001	0.042	83.3 ± 22.4	***
A3701-191120	Out-of-view	0.248	0.046	< 0.001	0.035	82.6 ± 23.8	***
	All data	-0.044	0.021	0.038	0.002	91.0 ± 64.5	*
	In-view	-0.330	0.038	< 0.001	0.110	72.8 ± 13.5	***
A3705-200307	Out-of-view	0.054	0.047	0.256	0.002	-	ns
	All data	-0.255	0.025	< 0.001	0.044	55.3 ± 10.3	***
	In-view	-0.516	0.080	< 0.001	0.121	75.1 ± 19.4	***
A3711-200815	Out-of-view	-0.009	0.186	0.963	0.000	-	ns
	All data	-0.227	0.084	0.007	0.005	74.0 ± 43.6	**
	In-view	-0.616	0.197	0.002	0.038	83.1 ± 38.2	**
A3711-200810	Out-of-view	-0.045	0.050	0.368	0.001	30.7 ± 106.1	ns
	All data	-0.214	0.036	< 0.001	0.017	90.8 ± 21.9	***
	In-view	-0.495	0.152	0.001	0.041	103.7 ± 43.0	**
A3712-200903b	Out-of-view	0.381	0.074	< 0.001	0.036	109.6 ± 27.8	***
	All data	0.069	0.040	0.082	0.001	196.5 ± 123.7	ns
	In-view	-0.620	0.089	< 0.001	0.055	76.8 ± 16.8	***

Table 4: Parallax Analysis Results - Multi-Cue. Anchoring angles with standard errors $> 180^\circ$ are not reported.

Session	Condition	w	SD	p-value	R^2	γ_{anchor} (deg)	Significance
A3701	Out-of-view	-0.089	0.017	< 0.001	0.044	50.1 ± 20.6	***
	All data	-0.032	0.010	0.002	0.006	59.4 ± 36.7	**
	In-view	0.129	0.026	< 0.001	0.063	83.9 ± 27.7	***
A3702	Out-of-view	-0.012	0.012	0.329	0.001	-	ns
	All data	-0.040	0.011	< 0.001	0.010	4.9 ± 24.3	***
	In-view	-0.044	0.024	0.067	0.012	94.8 ± 68.8	ns
A3703	Out-of-view	-0.033	0.010	0.001	0.013	96.7 ± 40.4	**
	All data	-0.016	0.008	0.050	0.002	88.3 ± 61.4	*
	In-view	0.001	0.028	0.983	0.000	-	ns
A3705	Out-of-view	0.060	0.024	0.011	0.015	136.7 ± 67.4	*
	All data	-0.031	0.012	0.009	0.005	-13.7 ± 38.7	**
	In-view	-0.194	0.019	< 0.001	0.210	76.4 ± 11.5	***
A3706	Out-of-view	-0.069	0.024	0.004	0.028	-38.6 ± 27.1	**
	All data	-0.072	0.010	< 0.001	0.035	-22.7 ± 13.0	***
	In-view	-0.138	0.016	< 0.001	0.111	42.6 ± 12.5	***
A3707	Out-of-view	-0.061	0.029	0.032	0.015	-5.1 ± 60.3	*
	All data	-0.077	0.014	< 0.001	0.051	36.6 ± 20.1	***
	In-view	-0.224	0.034	< 0.001	0.289	61.7 ± 16.0	***
A3708	Out-of-view	0.134	0.027	< 0.001	0.096	71.6 ± 24.0	***
	All data	0.090	0.019	< 0.001	0.027	67.9 ± 24.4	***
	In-view	-0.213	0.067	0.001	0.044	105.0 ± 44.9	**
A3710	Out-of-view	0.009	0.024	0.699	0.000	-	ns
	All data	-0.000	0.014	0.983	0.000	-	ns
	In-view	-0.060	0.019	0.002	0.013	67.5 ± 36.7	**
A3711	Out-of-view	0.031	0.026	0.231	0.003	115.2 ± 127.1	ns
	All data	0.034	0.020	0.093	0.003	64.2 ± 64.3	ns
	In-view	0.074	0.039	0.056	0.012	48.9 ± 54.6	ns
A3712	Out-of-view	0.078	0.041	0.061	0.008	183.8 ± 108.3	ns
	All data	-0.050	0.020	0.013	0.002	-10.7 ± 40.4	*
	In-view	0.007	0.054	0.900	0.000	-	ns
A3713	Out-of-view	-0.263	0.024	< 0.001	0.241	112.8 ± 14.5	***
	All data	-0.244	0.013	< 0.001	0.189	115.7 ± 8.2	***
	In-view	-0.248	0.026	< 0.001	0.210	125.2 ± 18.8	***
A3716	Out-of-view	0.188	0.058	0.001	0.042	106.4 ± 46.2	**
	All data	0.040	0.018	0.027	0.004	103.2 ± 66.1	*
	In-view	-0.024	0.027	0.376	0.002	112.8 ± 161.7	ns
A3717	Out-of-view	-0.010	0.027	0.719	0.000	-	ns
	All data	0.012	0.017	0.480	0.000	-	ns
	In-view	0.089	0.044	0.043	0.011	130.1 ± 77.6	*
A3723	Out-of-view	0.133	0.038	< 0.001	0.027	127.6 ± 43.2	***
	All data	-0.009	0.023	0.682	0.000	-	ns
	In-view	-0.153	0.032	< 0.001	0.030	80.1 ± 27.3	***
A3728	Out-of-view	-0.191	0.043	< 0.001	0.057	25.1 ± 19.6	***
	All data	-0.099	0.024	< 0.001	0.014	21.2 ± 26.1	***
	In-view	-0.076	0.084	0.365	0.006	116.5 ± 170.9	ns
A3730	Out-of-view	-0.061	0.026	0.020	0.017	88.1 ± 63.3	*
	All data	-0.046	0.011	< 0.001	0.012	66.4 ± 26.9	***
	In-view	-0.031	0.022	0.169	0.004	73.8 ± 77.1	ns

Supplementary plots for all sessions

In this section, we provide additional plots for all sessions in cases where we only showed example sessions in the main text.

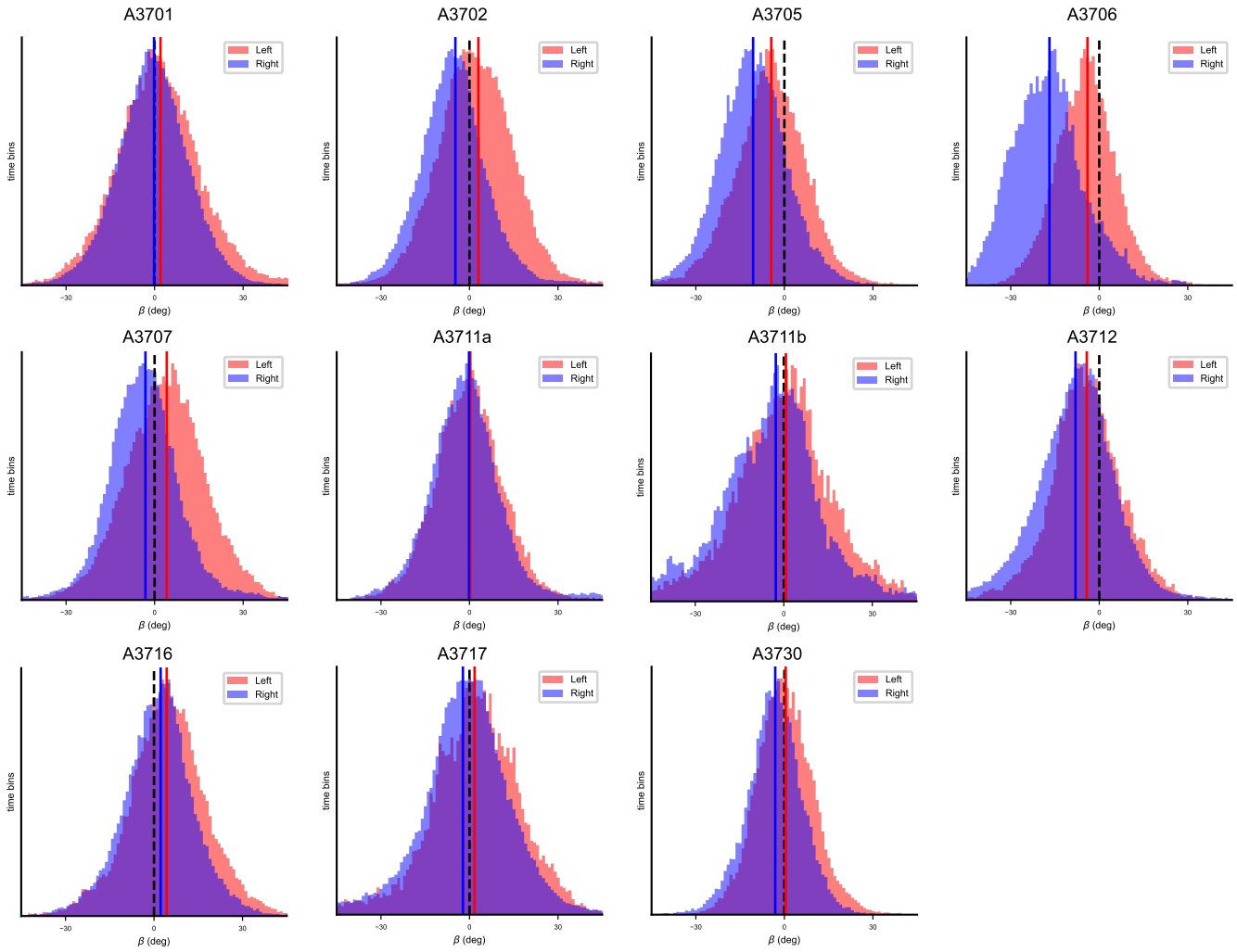

Figure 7: **Decoding error histogram split by left and right region in environment for single cue datasets.**

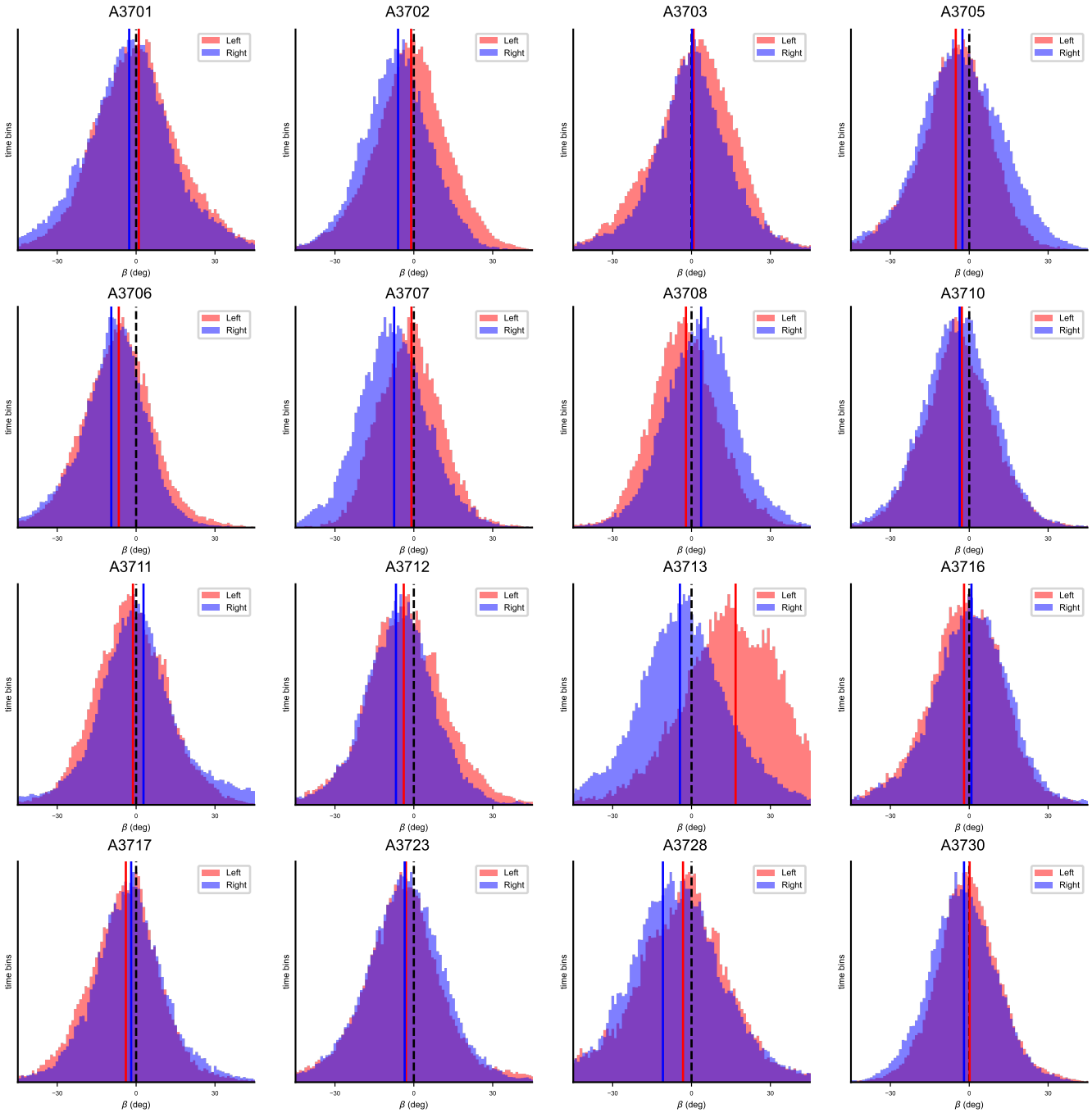

Figure 8: **Decoding error histogram split by left and right region in environment for multi-cue dataset.**

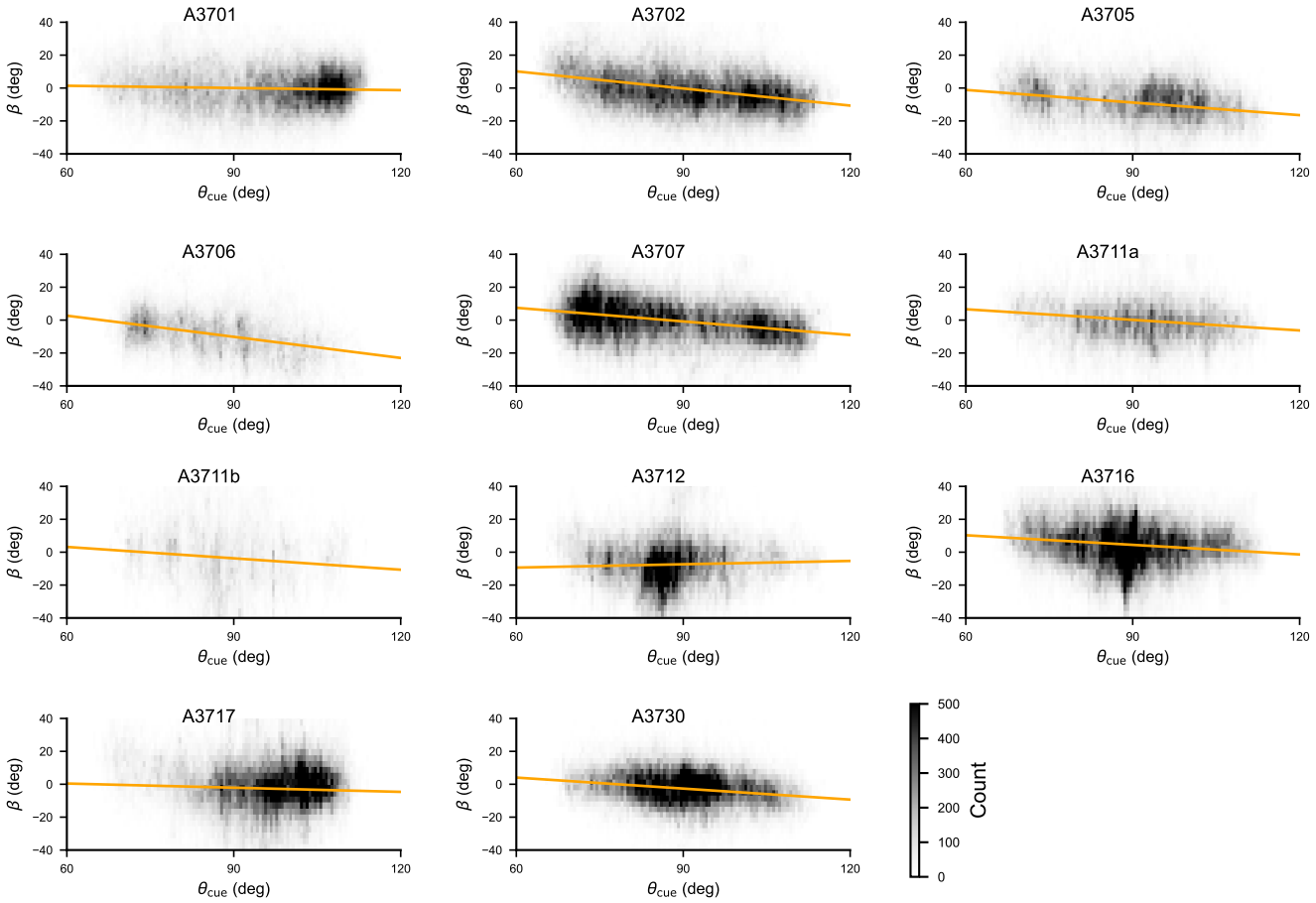

Figure 9: **Linear regression slopes for the single cue dataset.**

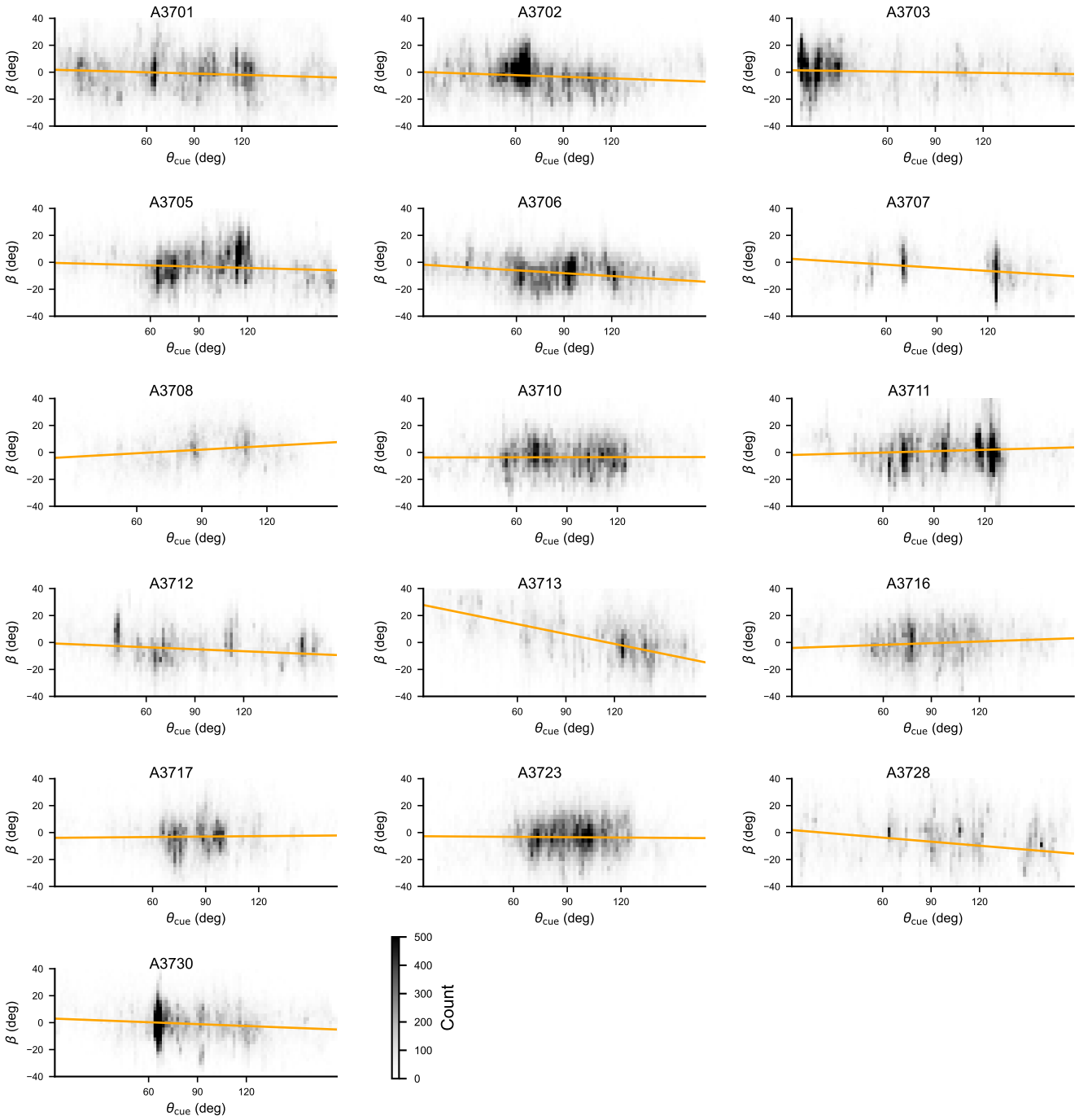

Figure 10: **Linear regression slopes for the multi-cue dataset.**

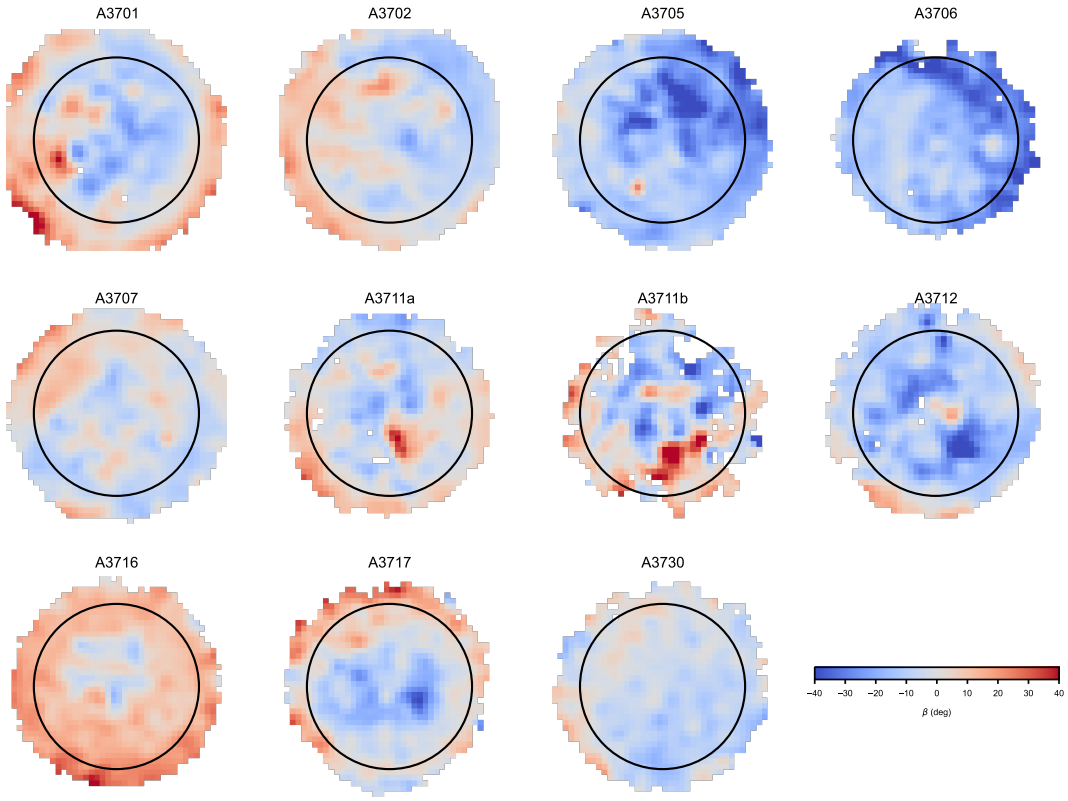

Figure 11: **Heat maps of measured parallax across space.** Same as Fig. 2, here for all sessions in the single cue dataset.

Supplementary plots for additional data overview

Here, we provide additional information plots that support the analysis described in the main text.

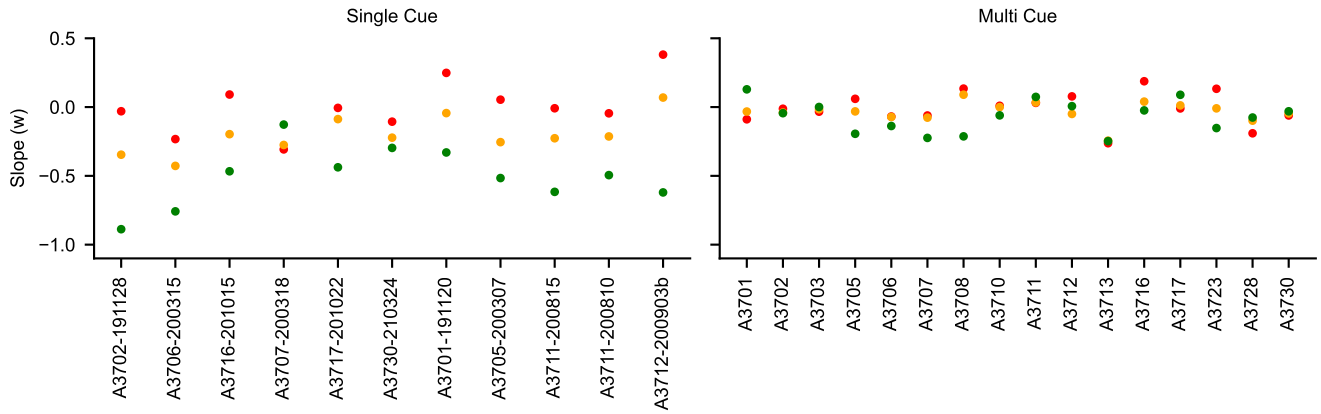

Figure 12: **Scatter plot of all slopes.** Slopes measured for all sessions in all three conditions (out-of-view (red), all data (orange), and in-view (green)). Shown for all sessions in the single cue dataset (left) and multi-cue dataset (right).

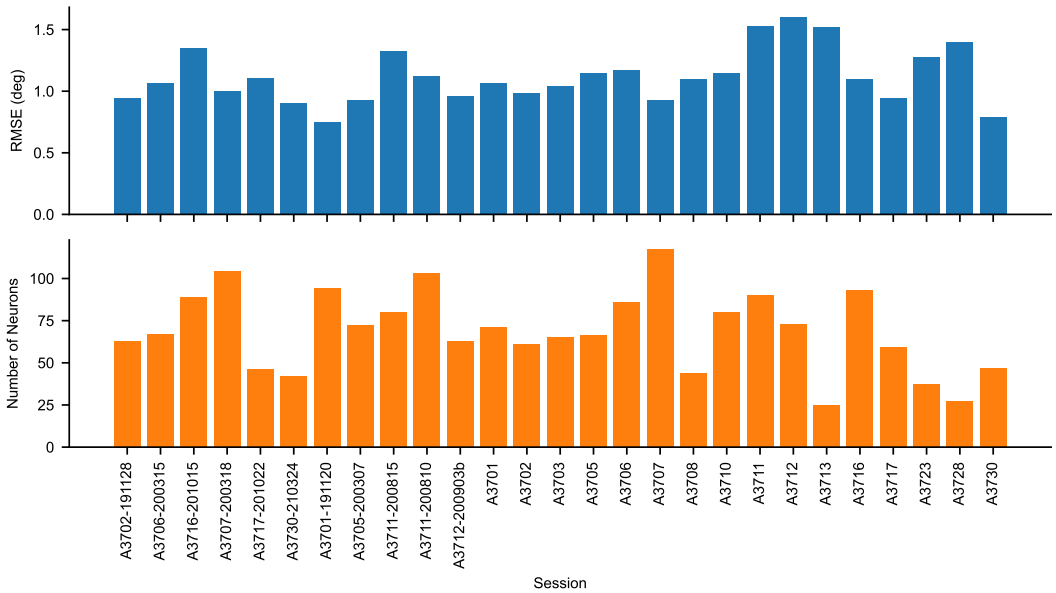

Figure 13: **Mean decoding error and number of neurons per session. (a)**: Bars show the root mean squared error between the tracked and decoded head direction. Switch periods and other rejected periods due to tracking errors are excluded from this data. **(b)**: Number of neurons recorded in each session.